Pump-probe optical coherence tomography using indocyanine green as a contrast agent

Zahid Yaqoob, Emily McDowell, Jigang Wu, Changhuei Yang

Zahid Yaqoob, Emily McDowell, Jigang Wu, Changhuei Yang, "Pump-probe optical coherence tomography using indocyanine green as a contrast agent," Proc. SPIE 6079, Coherence Domain Optical Methods and Optical Coherence Tomography in Biomedicine X, 607904 (20 February 2006); doi: 10.1117/12.646509

SPIE.

Event: SPIE BiOS, 2006, San Jose, California, United States

Pump-probe optical coherence tomography using indocyanine green as a contrast agent

Zahid Yaqoob, Emily McDowell, Jigang Wu, and Changhuei Yang

Biophotonics Laboratory, Department of Electrical Engineering
California Institute of Technology, Pasadena, CA 91125
Email: zyaqoob@caltech.edu

ABSTRACT

Use of indocyanine green (ICG), an FDA-approved dye, in a pump-probe scheme for optical coherence tomography (OCT) is reported. Aqueous solutions of ICG are not stable, i.e., the dye degrades over time especially in the presence of light. Addition of protein such as bovine serum albumin (BSA) stabilizes the ICG; however, when exposed to high intensity illumination, the dye still degrades. Moreover, the photodegradation is permanent and occurs swiftly if the illumination band corresponds to the ICG absorption peak. The permanence of the photobleached state illustrates that ICG photobleaching phenomenon has great potential to achieve contrast in OCT. ICG solutions with 50 μM concentration were prepared in water, 1% BSA, and 0.8% agarose to study the dynamics of the dye for different illumination intensity levels. In addition, different molar concentrations of ICG in water were studied for fixed illumination intensity. In each case, probability of photobleaching, defined as the ratio of the total photobleached ICG molecules to the total photons absorbed by the ground-state molecules, is evaluated to characterize the photobleaching phenomenon in ICG. We also demonstrate ICG-based pump-probe MCOCT imaging by mapping the distribution of ICG in a stage 54 *Xenopus laevis*.

Keywords: Optical coherence tomography, Indocyanine green, Medical and biological imaging, Pump-probe

1. INTRODUCTION

Optical coherence tomography[1] (OCT) is a vital non-invasive biomedical tool for high resolution imaging of biological samples to a depth of few millimeters. Since its inception, OCT has matured into a useful diagnostic tool for ophthalmic applications.[2, 3] OCT's applications for imaging other areas of the human body include endoscopic imaging of gastrointestinal (GI) tract [4] and bladder [5] for tumor detection, monitoring and risk assessment of vulnerable lipid plaques in the vascular system,[6] monitoring intracoronary stenting,[7] and tracking structural weakness associated with tooth decay.[8] While a basic OCT imaging method is able to render depth resolved structural images of the target, more sophisticated OCT imaging strategies can provide additional functional information such as flow (through Doppler OCT),[9] tissue structural arrangement (through birefringence OCT),[10] and depth resolved spectral signatures (through spectral OCT).[11, 12] Recently, a new and exciting type of functional OCT method, known as molecular contrast optical coherence tomography (MCOCT),[13-16] has been introduced that combines the major advantages of fluorescence microscopy (chemical contrast detection and imaging capability) and OCT (higher spatial resolution and depth penetration). MCOCT schemes reported so far can be categorized into three major groups; namely, absorption, coherent-emission, and scattering based MCOCT. This paper deals with a pump-probe MCOCT scheme that falls within the first category, i.e., absorption-based MCOCT.

In pump-probe MCOCT, a baseline OCT scan of the sample containing a contrast agent is first acquired, followed by photo-excitation of the contrast agent. The photo-illumination alters the absorption extinction coefficient of the contrast agent. A second OCT scan is then acquired. The two OCT scans are slightly different as the absorption spectrum of the contrast agent has changed. The two OCT scans are thus processed to determine the distribution of the contrast agent within the sample. The first reported pump-probe MCOCT scheme used methylene blue (MB) as the contrast agent.[13] Notice that the triplet state in MB has a life time of only ~2 μs, which requires very strong illumination intensity, e.g., > 10 MW/cm^2, of the pump source to achieve contrast. A contrast agent with higher absorption cross section and longer life time is therefore highly desirable. Recently, indocyanine green (ICG), which is frequently used in medical

Coherence Domain Optical Methods and Optical Coherence Tomography in Biomedicine X
edited by Valery V. Tuchin, Joseph A. Izatt, James G. Fujimoto, Proc. of SPIE Vol. 6079
607904, (2006) · 1605-7422/06/$15 · doi: 10.1117/12.646509

diagnostics[17] and photodynamic therapy,[18] was used as a contrast agent in an MCOCT implementation in which contrast agent's distribution inside the sample was determined from agent's spectral differential absorption.[16] Later, a pump-scheme for MCOCT was proposed using ICG as a contrast agent.[19] This paper extends on the same idea and provides better understanding of ICG dynamics in a pump-probe scheme. We also demonstrate the MCOCT technique in an animal model.

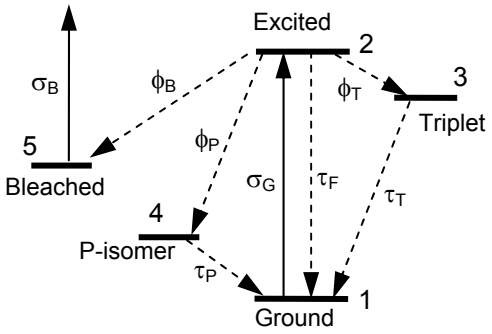

Figure 1: Schematic of electronic state diagram of ICG. σ_G is the ground state absorption cross section whereas ϕ_T, ϕ_P, and ϕ_B are quantum yields of triplet (T), P-isomer (P), and bleached (B) states.

In addition to the ground and first excited states, ICG has three more states of interest, namely the triplet (T), P-isomer (P), and bleached (B) states, in which the molecules can reside (see Fig.1). The quantum yields ϕ_T, ϕ_P, and ϕ_B of the three states are very small ($\sim 10^{-5} - 10^{-6}$),[20] so most of the excited state molecules relax directly back to the ground state (fluorescence signal). The life times of triplet and P-isomer states are small, i.e., τ_T ~700 μs and τ_P ~10 ms, respectively.[20] Low quantum yield and small life times indicate that triplet and P-isomer states cannot accumulate enough ICG molecules to deliver noticeable contrast. However, the photobleached state, with similarly low quantum yield, is permanent. This implies that, given enough time, all the molecules in an illuminated sample of ICG solution can be sent to the bleached state.

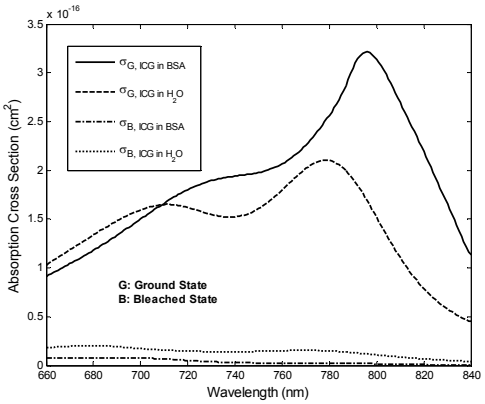

Figure 2: Absorption cross section spectra of unbleached as well as bleached samples of ICG in 1% BSA and water. ICG concentration is 50 μM in all the cases.

For the sake of substantiation, 1 cm path length glass cuvettes (from Starna Cells, Inc.) were filled with 50 μM ICG solutions in 1% bovine serum albumin (BSA) and water, and exposed to 790 nm illumination (incident optical power ~ 1.2 Watts) for several hours. Figure 2 shows absorption cross section spectra of both unbleached and bleached samples of 50 μM ICG solution in 1% BSA and water. The absorption cross section spectra of the bleached samples of ICG in 1% BSA and water showed no signs of recovering, confirming that the photobleached state is permanent. The permanence of photobleaching illustrates the usefulness of this transition in a pump-probe scheme for OCT – a focus of this study.

2. DEGRADATION DYNAMICS OF INDOCYANINE GREEN

Figure 3 shows a setup to study the degradation dynamics of ICG. A fraction of the collimated beam from the light source (Ti:Sapphire laser) is split off using a beam splitter (BS) to form the reference beam. The major portion of the light, i.e., the signal beam passes through a small self-assembled 1.52 mm path length circular cuvette, 1.98 mm in diameter. The diameter of the collimated laser beam is approximately the size of the circular cuvette diameter. A balanced photodetector (New Focus, Inc.) is used to measure the transmission through the ICG samples versus time.

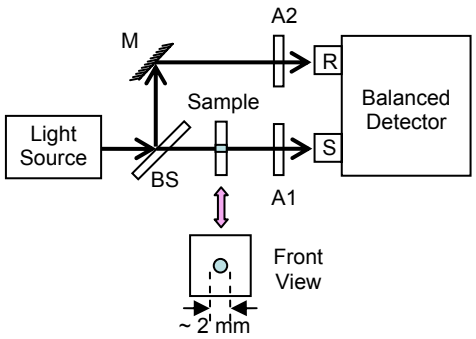

Figure 3: Experimental setup to study ICG photodegradation dynamics. M: Mirror; BS: Beamsplitter; A: Attenuator; R: Reference beam; S: Sample beam.

First, ICG (product # SDB8662, acquired from H. W. Sands Corp.) was used to prepare 50 μM solutions in deionized (DI) water, 1% BSA, and 0.8% agarose to study ICG sample transmission versus time for different illumination intensities. Note that before each transmission measurement, the system was balanced by using the corresponding solvent (water, 0.8% agarose, or 1% BSA) in an identical cuvette and adjusting the free-space attenuators A_1 and A_2 accordingly. Figure 4 shows the transmission curves of 50 μM ICG in water, 1% BSA, and 0.8% agarose for different illumination intensities.

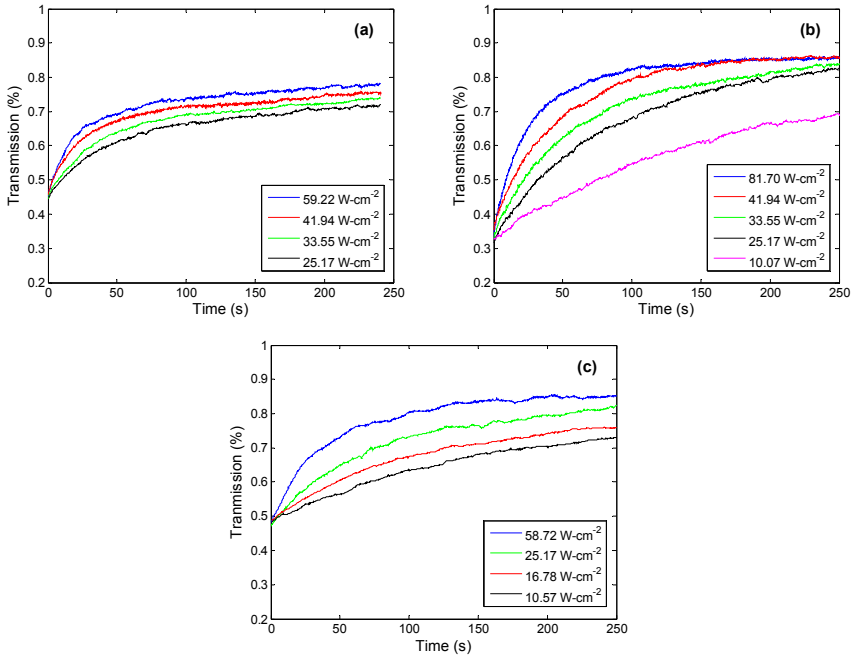

Figure 4: Transmission curves for 50 μM ICG versus time in (a) DI water, (b) 1% BSA, and (c) 0.8% agarose for different illumination intensities. Note that fresh samples of ICG were used for different illumination intensities of the laser.

The quantum yield of the bleached state may also be thought of as the probability of photobleaching, ϕ_B, defined as the ratio of total number of photobleached molecules to the total number of photons absorbed by ground state molecules. Considering only ground, excited, and photobleached states (see Fig. 1), the bleached state population density $N_B(t)$ can be written in terms of transmission $T(t)$ as:

$$N_B(t) = \frac{1}{(\sigma_G - \sigma_B)L} \ln\left[\frac{T(t)}{T_{\min}}\right], \qquad (1)$$

where L is the sample path length and $T_{\min} = \exp\{-\sigma_G N_0 L\}$ is the minimum transmission at $t = 0$. For a 50 μM ICG concentration, N_0, the number of ICG molecules per unit volume, is 3.011×10^{16} cm^{-3}. Because the illumination intensity decays through the sample, $N_B(t)$ represents spatial average of the bleached state population density varying with exposure time. Therefore, the probability of photobleaching, ϕ_B, can be mathematically written as:

$$\phi_{B,\text{cum}}(t) = \frac{N_B(t)\times V}{\left(1 - \frac{N_B(t)}{N_0}\right)\int \frac{P_0 - P(t)}{h\nu} dt}, \qquad (2)$$

where V is the volume of the ICG sample, h is Planck's constant, ν is the optical frequency of illumination, P_0 is the incident optical power, and $P(t) = P_0 \times T(t)$ is the transmitted power. The term $(1 - N_B(t)/N_0)$ assures that only the photons absorbed by the ground state ICG molecules are considered. It can be seen from Eq. (2) that the probability of photobleaching, $\phi_B(t)$, is a function of time. Moreover, $\phi_B(t)$ determined in this fashion yields a probability which is cumulative in nature such that at a given time t', $\phi_{B,\text{cum}}(t')$ gives an average probability of photobleaching for time interval $[0, t']$.

The transmission data shown in Fig. 4 were processed to determine probability of photobleaching using Eqs. (1) and (2). It was found that the probability of photobleaching in ICG does change with exposure time. However, it does not vary significantly with the illumination intensity. For each sample of ICG (in water, BSA, and agarose), the probability curves for different illumination intensity were averaged; Figs 5 (a) shows average $\phi_{B,\text{cum}}(t)$ curve for 50 μM ICG in water. This empirical study shows that probability of photobleaching, $\phi_{B,\text{cum}}(t)$, decreases with exposure time.

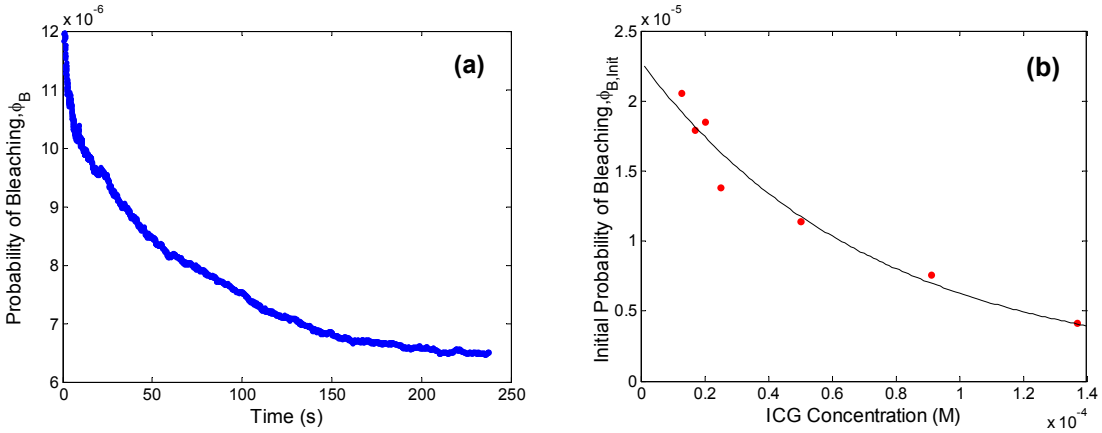

Figure 5: (a) Average $\phi_{B,\text{cum}}(t)$ curves for 50 μM ICG in DI water. (b) Initial probability of photobleaching $\phi_{B,\text{cum,init}}$ [determined using Eq. (2)] versus ICG concentration. The illumination intensity is 33.55 W/cm^2.

We also studied the photobleaching phenomenon in various other concentrations of ICG in DI water. To keep the initial transmissions alike for different concentrations of ICG, glass cuvettes with different path lengths were assembled in our laboratory. ICG concentrations ranging from 12 μM to 137 μM were used in the study. The input illumination intensity on each sample was ~33.55 W/cm^2. For each concentration, several sets of measurements were acquired to assure accuracy. The transmission curves were processed to determine probability of photobleaching versus time, using the

cumulative approach defined by Eq. (2). The initial probability of photobleaching $\phi_{B,cum,init}$ versus ICG concentration is shown in Fig. 5(b), where a decrease in $\phi_{B,cum,init}$ with increasing dye concentration can be clearly seen. Note that curve fitting the data in Fig. 5(b) with a decaying exponential can be used to estimate initial probability of photobleaching for higher concentrations of ICG. This study shows that samples of ICG prepared in higher concentrations are more stable than the one prepared in lower concentrations.

3. PUMP-PROBE MOLECULAR CONTRAST OPTICAL COHERENCE TOMOGRAPHY SETUP

Figure 6(a) shows a fiber-optic spectral domain MCOCT setup that uses a high power broadband laser such as a Ti:Sapphire. A programmable fiber-optic attenuator (PFOA) realized using a galvanometer-based mirror scanner controls the amount of light reaching the sample during ICG photobleaching as well as OCT signal acquisition. A personal computer both controls the PFOA and acquires data from the spectrometer. From operational point of view, the PFOA is first set to deliver low optical power, usually less than 100 μW, so that ICG is as little photobleached as possible during the first OCT scan. After the first OCT scan is acquired at time t_1, the PFOA is set to deliver high power, usually 1000×, for set duration Δt to photobleach the ICG. The optical power transmitted by the PFOA is then reduced to the same level as for the first OCT scan to acquire the second OCT scan at time t_2. The timing diagram of the pump-probe scheme is shown in Figure 6(b).

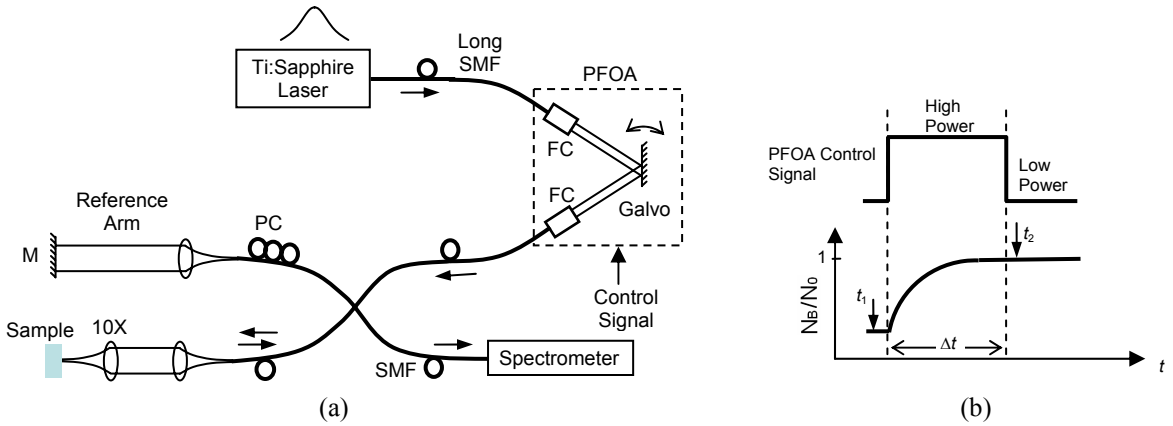

Figure 6: (a) Proof- of- concept pump-probe MCOCT setup. PC: Polarization controller, SMF: Single mode fiber; PFOA: Programmable fiber-optic attenuator, FC: Fiber collimator. (b) Timing diagram for pump-probe scheme.

At the interferometer, the light collected from the reference and sample arms is spectrally dispersed using a diffraction grating and detected using *N* different detectors. For the spectral domain MCOCT setup shown in Fig. 6(a), the spectrally resolved interferometric OCT signal can be mathematically expressed as:

$$P_{\text{interferemce}}(k,z) = 2\,S(k)\,\eta(k)[1-\eta(k)]\sqrt{R_R}\sqrt{R_s(\lambda,z)} \times e^{-\int_0^z [\mu_a(\lambda,z_s')+\mu_s(\lambda,z_s')]dz_s'} \cos[2\pi\, k\,(z-z_r)], \quad (3)$$

where k is the optical wavenumber, S(k) is the source spectral profile, $\eta(k)$ is optical power split factor of the 2×2 coupler (½ in an ideal case), R_R is the reflectivity of the reference mirror, $R_s(\lambda,z)$ is the sample reflectivity at depth z, and $(z-z_r)$ is the path length difference between the reference arm mirror and the plane of interest inside the sample. $\mu_a(\lambda,z)$ and $\mu_s(\lambda,z)$ are the absorption and scattering coefficients, respectively, of the sample. In a pump-probe scheme such as the one discussed above using ICG as the contrast agent, the photo-illumination permanently alters the absorption coefficient of the dye. In this context, the absorption coefficient can be mathematically written as:

$$\mu_a(\lambda,z) = \mu_{a,\text{intrinsic}}(\lambda,z) + \mu_{a,\text{ICG\_ground}}(\lambda,z) + \Delta\mu_{a,\text{ICG}}(\lambda,z), \quad (4)$$

where $\mu_{a,\text{intrinsic}}(\lambda,z)$ is the localized intrinsic absorption coefficient of the sample, $\mu_{a,\text{ICG\_ground}}(\lambda,z)$ is the localized absorption coefficient component for ICG in the ground state, and $\Delta\mu_{a,\text{ICG}}(\lambda,z)$ is the change in the absorption coefficient between the two OCT scans. The two quantities, $\mu_{a,\text{ICG\_ground}}(\lambda,z)$ and $\Delta\mu_{a,\text{ICG}}(\lambda,z)$, can be expressed as:

$$\mu_{a,\text{ICG\_ground}}(\lambda,z) = \sigma_G(\lambda)N_0(z), \quad (5)$$

$$\Delta\mu_{a,\text{ICG}}(\lambda,z) = \left[\sigma_G(\lambda)N_G(z) + \sigma_B(\lambda)N_B(z)\right] - \sigma_G(\lambda)N_0(z). \quad (6)$$

where $\sigma_G(\lambda)$ and $\sigma_B(\lambda)$ are the ground and bleached state absorption cross section spectra, respectively. $N_0(z)$ is the initial ground state population density of ICG, whereas $N_G(z)$ and $N_B(z)$ are the ground and bleached state population densities when the second OCT scan is acquired. Since the lifetime of ICG molecules in the excited state is extremely small (~ in ps), we can safely assume that $N_0(z) = N_G(z) + N_B(z)$. Therefore, Eq. (6) can be simplified as:

$$\Delta\mu_{a,\text{ICG}}(\lambda,z) = \left[\sigma_B(\lambda) - \sigma_G(\lambda)\right]N_B(z). \quad (7)$$

If $P_{\text{interference\_ground}}(\lambda,z)$ and $P_{\text{interference\_bleached}}(\lambda,z)$ are the OCT signals acquired before and after the photobleaching of ICG, the change in absorption coefficient is related to the two OCT scans by:

$$\int_0^z \Delta\mu_{a,\text{ICG}}(\lambda,z')\,dz' = -\ln\left[\frac{P_{\text{interferernce\_bleached}}(k,z)}{P_{\text{interferernce\_ground}}(k,z)}\right]. \quad (8)$$

4. EXPERIMENT

A spectral domain MCOCT system similar to that shown in Fig. 6(a) was realized for demonstration. Light from a modelocked Ti:Sapphire laser (~12 nm FWHM) is coupled into a long 5/125 μm SMF for spectrum broadening. Broadband probe light (~60 nm FWHM centered at 800 nm) reaches the 2×2 single mode fiber-optic coupler via a galvo-based PFOA. Light from the coupler is collimated by lens L_1 (f_1 = 11mm) and focused onto the sample by a 10× microscope objective lens (f_2 = 16.5 mm). The calculated $1/e^2$ focal spot size on the sample is 8.24 μm, which corresponds to a depth of focus of 135 μm. Light collected from the two arms of the interferometer is detected by a spectrometer designed and built in our laboratory, which features 0.07 nm spectral resolution. The spectral oscillation data acquired by the spectrometer are first rescaled and resampled evenly in *k*-space, before it is Fourier transformed to retrieve the sample depth profile (or A-scan). Our laboratory MCOCT system features a base SNR of ~90 dB at 0.8 millisecond integration time.

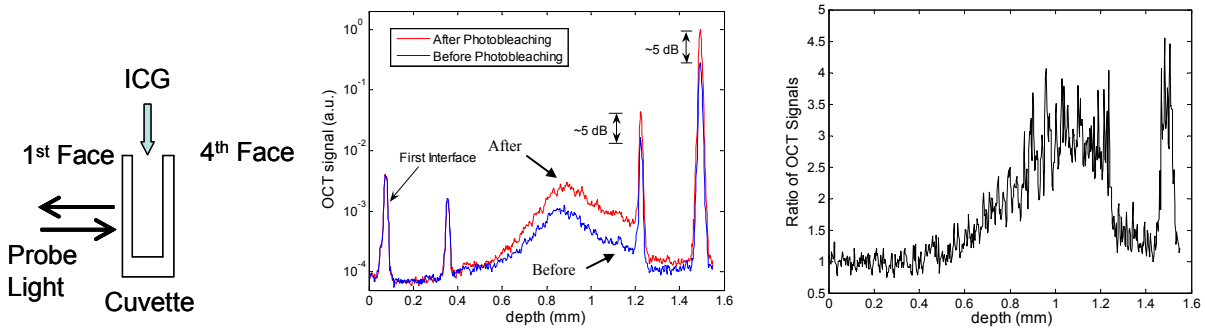

(a) (b) (c)

Figure 7: (a) Side view of a self-assembled 0.84 mm path length glass cuvette. (b) A-scans of the glass cuvette filled with a mixture of 200 μM ICG and 0.25% volume concentration 0.1-μm latex microspheres before and after the photobleaching. (c) Ratio of the two A-scans is shown in Fig. 7(c).

In a proof-of-concept demonstration, a self assembled 0.84 mm path length glass cuvette, filled with a mixture of 200 μM ICG and 0.25% (v/v) 0.1-μm latex microspheres, was used as a sample [see Fig. 7(a)]. The galvo-based PFOA was programmed to deliver 68 μW and 10 mW optical power levels on the sample for OCT signal acquisition and ICG photobleaching, respectively. The ICG was photobleached for duration Δt = 2.5 seconds between the two OCT scans. Figure 7(b) shows averaged A-scans of the glass cuvette before (blue) and after (red) the photobleaching. The first two interfaces show no contrast as anticipated. The last two interfaces of the glass cuvette yield a measured contrast of ~ 5 dB. Notice that the contrast increases with ICG sample depth as it is cumulative in nature [see Eq. (8)]. A ratio of the two averaged A-scans is shown in Fig. 7(c) to support the argument.

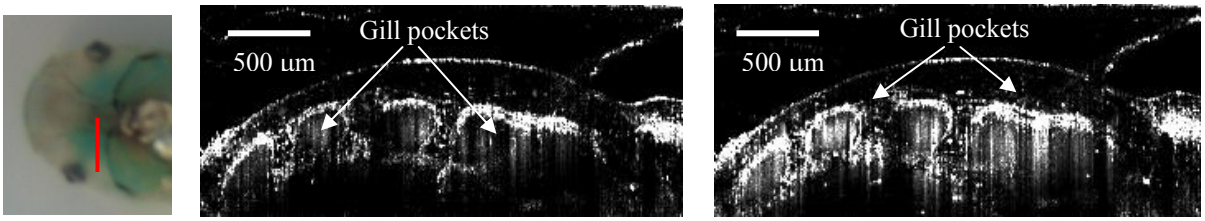

(a) (b) (c)

Figure 8: MCOCT imaging of a stage 54 *Xenopus laevis*. (a) Ventral view of *Xenopus laevis* filled with a mixture of 400 μM ICG and 0.25% - 0.1μm latex microspheres; the red line indicates the region where OCT scans were acquired. (b) and (c) show B-scans of the illuminated region before and after ICG photobleaching, respectively.

To demonstrate the ICG detection capability in an animal model, a mixture of 400 μM ICG, ~0.25% volume concentration 0.1 μm latex microspheres, and 0.6% volume concentration of agarose was filled in gill arch cavities of euthanized stage 54 *Xenopus laevis*. First, the PFOA was set to illuminate the sample with ~60 μW and a whole B-scan (400 A-scans; lateral resolution ~7.5 μm) was acquired by moving the sample using a linear stage [see Fig. 8(b)]. During the second B-scan, the PFOA was set to illuminate the sample with ~10mW power at each A-scan position for 12 sec duration. The optical power was then readjusted to ~60 μW to acquire the corresponding A-scan, and so forth. Figure 8(c) shows the second B-scan where increased backscatter from the microspheres (indicating the localization of ICG) in gill arch cavities can be clearly seen. This increased backscatter, attributable to change in the absorption coefficient of ICG from within the gill arch cavities of the tadpole, demonstrates the functionality of ICG as contrast agent in the proposed pump-probe MCOCT scheme.

5. CONCLUSION

In conclusion, we have conducted a study of ICG photobleaching in water, BSA, and agarose. The study indicates that the photobleached state is permanent, which makes this transition useful in a pump-probe scheme for OCT. Exposure of ICG solutions in DI water, BSA, and agarose with different illumination intensity levels shows that the probability of photobleaching decreases with exposure time in all the cases. The study of various concentrations (ranging from 12 μM to 137 μM) of ICG in DI water for a fixed illumination intensity illustrates that the initial probability of photobleaching also decreases with increasing concentration. This information can be used to estimate the initial probability of photobleaching for higher concentrations, which helps understand the dynamics of ICG when used as a contrast agent in a pump-probe MCOCT scheme. Using our laboratory spectral domain MCOCT setup, which utilizes a Ti:Sapphire laser coupled to a galvo-based PFOA, we have successfully demonstrated, for the first time, ICG-based pump-probe MCOCT by mapping the dye distribution within gill arch cavities of a stage 54 *Xenopus laevis*. We strongly believe that the ability of ICG to provide high contrast in pump-probe MCOCT, combined with its high affinity to bind with proteins, and FDA approval for use in humans, can help realize an exciting functional imaging modality providing both high resolution, depth-resolved, structural information of tissue, as well as the ability to differentiate between certain tissue pathologies. In future, we plan to investigate other molecular contrast agents, specifically with higher probability of bleaching as well as larger absorption cross section, for use in our pump-probe MCOCT scheme.

Acknowledgement: This research was supported by National Institute of Health (NIH) grant 1RZ1EB004602-1

REFERENCES

1. Huang D, Swanson EA, Lin CP, et al. Optical Coherence Tomography. Science 1991;254(5035):1178-81.
2. Hee MR, Izatt JA, Swanson EA, et al. Optical Coherence Tomography of the Human Retina. Archives of Ophthalmology 1995;113(3):325-32.
3. Targowski P, Wojtkowski M, Kowalczyk A, et al. Complex spectral OCT in human eye imaging in vivo. Optics Communications 2004;229(1-6):79-84.
4. Rollins AM, Ung-arunyawee R, Chak A, et al. Real-time in vivo imaging of human gastrointestinal ultrastructure by use of endoscopic optical coherence tomography with a novel efficient interferometer design. Optics Letters 1999;24(19):1358-60.
5. Xie TQ, Zeidel ML, Pan Y. Detection of tumorigenesis in urinary bladder with optical coherence tomography: optical characterization of morphological changes. Optics express, 2002; v. 10.
6. Tearney G, Bouma B. Atherosclerotic plaque characterization by spatial and temporal speckle pattern analysis. Optics Letters 2002;27(7):533 -5.
7. Bouma BE, Tearney GJ, Yabushita H, et al. Evaluation of intracoronary stenting by intravascular optical coherence tomography. Heart 2003;89(3):317-20.
8. Wang XJ, Milner TE, de Boer JF, et al. Characterization of dentin and enamel by use of optical coherence tomography. Applied Optics 1999;38(10):2092-6.
9. White B, Pierce M, Nassif N, et al. In vivo dynamic human retinal blood flow imaging using ultra-high-speed spectral domain optical Doppler tomography. Optics Express 2003;11(25):3490 -7.
10. Everett MJ, Schoenenberger K, Colston BW, Da Silva LB. Birefringence characterization of biological tissue by use of optical coherence tomography. Optics Letters 1998;23(3):228-30.
11. Morgner U, Drexler W, Kartner FX, et al. Spectroscopic optical coherence tomography. Optics Letters 2000;25(2):111-3.
12. Leitgeb R, Wojtkowski M, Kowalczyk A, et al. Spectral measurement of absorption by spectroscopic frequency-domain optical coherence tomography. Optics Letters 2000;25(11):820 - 2.
13. Rao KD, Choma MA, Yazdanfar S, et al. Molecular contrast in optical coherence tomography by use of a pump-probe technique. Optics Letters 2003;28(5):340-2.
14. Vinegoni C, Bredfeldt JS, Marks DL, Boppart SA. Nonlinear optical contrast enhancement for optical coherence tomography. Optics Express 2004;12.
15. Yang CH, Choma MA, Lamb LE, et al. Protein-based molecular contrast optical coherence tomography with phytochrome as the contrast agent. Optics Letters 2004;29(12):1396-8.
16. Yang CH, McGuckin LEL, Simon JD, et al. Spectral triangulation molecular contrast optical coherence tomography with indocyanine green as the contrast agent. Optics Letters 2004;29(17):2016-8.
17. Nimura H. Infrared ray electronic endoscopy combined with indocyanine green injection for detection of sentinel nodes of patients with gastric cancer. The British journal of surgery 2004;91(5):575-9.
18. Piccolino FC, Eandi CM, Ventre L, et al. Photodynamic therapy for chronic central serous chorioretinopathy. Retina-the Journal of Retinal and Vitreous Diseases 2003;23(6):752-63.
19. Yaqoob Z, Wu J, Fingler JP, et al. Pump-probe scheme for optical coherence tomography using Indocyanine Green mixed with albumin or human plasma. Conference on Lasers and Electro-Optics (CLEO 2005), Paper No. CFA3, 22-27 May (2005), Baltimore MD.
20. Gratz H, Penzkofer A, Abels C. Photo-isomerisation, triplet formation, and photo-degradation dynamics of indocyanine green solutions. Journal of photochemistry and photobiology. A, Chemistry 1999;128(1-3):101-9.